Fully-Automated Identification of Brain Abnormality From Whole Body FDG PET Imaging by Deep-Learning Based Brain Extraction

Wonseok Whi
Seoul National University
Hongyoon Choi (chy1000@snu.ac.kr)
Seoul National University Hospital
Jin Chul Paeng
Seoul National University Hospital
Keon Wook Kang
Seoul National University Hospital
Dong Soo Lee
Seoul National University Hospital
Gi Jeong Cheon
Seoul National University Hospital

Original research

Keywords: brain segmentation, quantitative PET analysis, deep learning, convolutional neural network, FDG-PET, brain FDG-PET

Posted Date: May 11th, 2021

DOI: https://doi.org/10.21203/rs.3.rs-475171/v1

Abstract

Background: The whole brain is often covered in [^{18}F]Fluorodeoxyglucose Positron emission tomography ([^{18}F]FDG-PET) in oncology patients, but the covered brain abnormality is typically screened by visual interpretation without quantitative analysis in clinical practice. In this study, we aimed to develop a fully automated quantitative interpretation pipeline of brain volume from an oncology PET image.

Method: We retrospectively collected five hundred oncologic [^{18}F]FDG-PET scans for training and validation of the automated brain extractor. We trained the model for extracting brain volume with two manually drawn bounding boxes on maximal intensity projection (MIP) images. ResNet-50, a convolutional neural network (CNN) was used for the model training. The brain volume was automatically extracted using the CNN model and spatially normalized. As an application of this automated analytic method, we enrolled twenty-four subjects with small cell lung cancer (SCLC) and performed voxelwise two-sample T-test for automatic detection of metastatic lesions.

Result: The deep learning-based brain extractor successfully identified the existence of whole-brain volume, with the accuracy of 98% for the validation set. The performance of extracting the brain measured by the intersection-over-union (IOU) of 3-D bounding boxes was 72.9±12.5% for the validation set. As an example of the application to automatically identify brain abnormality, this approach successfully identified the metastatic lesions in three of the four cases of SCLC patients with brain metastasis.

Conclusion: Based on the deep-learning based model, the brain volume was successfully extracted from whole-body FDG PET. We suggest this fully automated approach could be used for the quantitative analysis of brain metabolic pattern to identify abnormality during clinical interpretation of oncologic PET studies.

Background

[^{18}F]fluorodeoxyglucose Positron emission tomography ([^{18}F]FDG-PET) has been playing a crucial role in tumor imaging [1, 2]. The clinical implications include diagnosis of unknown tumor, staging, monitoring for recurrence, and clinical assessment of therapy [3]. The routine protocol for oncologic ^{18}F-FDG PET is so-called “torso” imaging, covering from skull base to mid-thigh in most of the PET centers [4]. However, in practice, covering the whole level of skull is often clinically useful, for example, assessment of brain metastasis in the high-prevalence type of tumor, such as lung cancer [5-7] . The covered brain volume is typically analyzed by visual inspection in clinical practice, due to low sensitivity in metastatic lesions compared with magnetic resonance (MR) imaging [8]. Thus, in the clinical setting, more effort is made to find the lesions of the body, not the brain, in oncology PET. However, incidental brain metastasis is important for clinical decision. Furthermore, brain metabolism reflecting functional activity is affected by chemotherapy as well as tumors themselves – e.g., paraneoplastic encephalitis, which could affect outcome [9, 10] . As a functional image that assesses the metabolism of the whole body as well as

tumors, quantitative information of covered brain extracted from the oncology FDG-PET study could be utilized to identify brain abnormality as well as unexpected metastasis. More specifically, with the aid of automated analytic methods, such as statistical parametric mapping (SPM) [11, 12], the information from brain PET images might improve sensitivity for detecting incidental brain disorders by measuring regional metabolic abnormalities [13], such as local-onset seizures [14], or Alzheimer's disease (AD) [15], as well as brain metastasis [16].

In this study, we aimed to develop a fully automatic quantitative analysis pipeline of brain volume from a given oncology PET image. To achieve this goal, deep learning models were exploited to detect the location of the brain and to identify whether a given PET study included whole brain. The detected brain was cropped and spatially normalized to the template brain. The automatically extracted and normalized brain volume could be used to perform statistical analysis including SPM. As an example, we applied this model to identify brain metastasis from whole body FDG PET imaging.

Methods

Subjects

For the training and validation data of the automatic brain extractor, five hundred whole body [^{18}F]FDG-PET scans were retrospectively collected. These PET scans were performed from June to July 2020 in a single center (Age = 66.7 ± 3.4, M : F = 194 : 306). The scans which were explicitly prescribed to include the brain (by the oncologic clinicians) were excluded from analysis, to remove the bias in the evaluation of detecting accuracy of brain existence. Among the 500 cases, the primary site of malignancy was breast (19.8%), lung (18.6%), hematologic (14.2%), colorectal (9.4%), biliary (6.8%), ovary (5.4%), pancreas (5.2%), liver (5.0%), stomach (4.2%), thymus (3.6%), urinary tract (3.4%), soft tissue (3.0%), thyroid (0.6%) or unknown (0.8%).

For the quantitative assessment of the extracted brain as an independent test, FDG PET images acquired from small-cell lung cancer (SCLC) patients were retrospectively collected. The scans were acquired from January 2014 to December 2017 in the same institute. To test whether our automated brain analysis pipeline identify brain metastasis in SCLC patients, groups were defined according to the presence of brain metastasis. Four patients had brain metastasis confirmed by brain MRI at baseline and follow-up (age: 66.8 ± 6.5, M : F = 4 : 0). Twenty PET scans without brain metastasis according to the baseline brain MRI were regarded as controls (age: 71.2 ± 6.1; M : F = 17 :3).

Image acquisition

As a routine protocol of FDG PET, after fasting more than 4 hours, patients were intravenously injected with 5.18 MBq/kg of FDG. After 1 hour, PET image was acquired from the skull base to the proximal thigh using dedicated PET/CT scanners (Biograph mCT 40 or mCT 64, Siemens, Erlangen, Germany) for 1 minute per bed. A Gaussian filter (FWHM 5 mm) was applied to reduce noise, and images were reconstructed using an ordered-subset expectation maximization algorithm (2 iterations and 21 subsets).

Deep learning model and training data for the brain extraction

We devised an automatic brain extractor, based on the following two objectives: 1) the evaluation of whether a scan included the entire brain and 2) establishment of 3-dimensional bounding box which included brain volume. To achieve these goals, we implemented a CNN-based deep-learning model, according to the following procedure. The brief outline of the study is shown in (**Fig. 1**).

For training of the model, the maximum intensity projection (MIP) image for each of the PET scan was generated. For each of the 500 MIP image, 2-dimensional bounding boxes were manually drawn on the anterior and lateral views of the MIP image. Coordinates from the two bounding boxes were merged to obtain coordinates of 3-dimensional bounding box for each PET image. Images that did not contain full range of brain was classified elsewhere, as “not containing entire brain”.

Two MIP images, anterior and lateral views, were changed to square matrices by zero-padding. The matrices were changed to 224 x 224 using bilinear interpolation. The pixel values represented standardized uptake value (SUV). To be inputs of a CNN model, pixel values were divided by 30, as most voxel values of PET volume has less than SUV 30 except urine, and then multiplied by 255 to have a range approximately 0 to 255.

We utilized ResNet-50 [17, 18] for the learning model, a convolutional neural network pre-trained with images from ImageNet database [19]. ResNet-50 was implemented for preprocessing of the input data and predicting the coordinates of 3-D bounding boxes from the MIP images. The pre-trained ResNet-50 respectively extracted feature vectors from the two views of MIP images. The extracted features were concatenated. Additional fully-connected layer with 4096 dimensions was connected to the concatenated feature vectors and then finally connected to different outputs. An output represented coordinates of bounding box of the brain consisting of 6-dimensional vectors (coordinates for 3 axes and width, length, and depth of the bounding box for 3 axes). Another output with one-dimensional vector that represented whether a given PET volume included the entire brain. Image augmentation was applied to the training dataset. MIP images were randomly augmented by multiplying voxel values, changing contrast, scaling and translating images.

We performed the internal validation by randomly selected 10% of the data as a validation set. The loss function was defined by two terms:

$$\mathrm{L}_a = Y_i \log\big(p(y)\big) + (1 - Y_i)\log\,(1 - p(y))$$

$$\mathrm{L}_b = \sum_{j=x,y,z,w_x,w_y,w_z} (y_{b,j} - \hat{y}_{b,j})^2$$

$$L_{all} = \alpha L_a + \beta L_b$$

1) binary cross entropy of an output that represented whether a given PET volume included the entire brain and 2) mean squared error estimated by the 6-dimensional vector representing coordinates of the bounding box (**Fig. 1**). The weight for the loss was changed according to the training process: we set to alpha = 10 and beta = 1 for the sum of loss function. We measured intersection over union (IOU) for the predicted and labeled bounding boxes. From the predicted coordinates of bounding boxes, we extracted brain images from whole body PET and spatially normalized them to the template space, as mentioned later.

Processing of the extracted brain

The trained model was applied to whole body PET images to extract brain if the model predicted that the image contains the whole brain volume. FDG PET volumes were resliced to have a voxel size of 2 x 2 x 2 mm^3. We segmented the brain with the coordinates of the 3-D bounding boxes predicted by the model. Padding of 10 voxels is applied for each axis to determine the brain volume. The extracted brain volumes were spatially normalized onto Montreal Neurological institute (McGill University, Montreal, Quebec, Canada) standard templates. The spatial normalization was performed by symmetric normalization (SyN) with the cross-correlation loss function implanted in DIPY package [20]. More specifically, a given extracted brain volume was linearly transformed to the template PET image with affine transform. The warping was performed by the symmetric diffeomorphic registration algorithm. The spatially normalized PET volume was saved for further quantitative imaging analysis.

Quantitative analysis of the extracted brain

The extracted and spatially normalized brain volume was analyzed by a quantitative software, SPM12 (Institute of Neurology, University College of London, London, U. K.) implemented in Matlab 2019b (The MathWorks, Inc., Natick, MA, U. S.). The normalized brain images were smoothed by convolution with an isotropic gaussian kernel having a 10 mm full width at half maximum to increase the signal-to-noise ratio.

For the twenty-four subjects with SCLC, we performed the voxelwise two-sample T-test for each of the normalized brain volume from the four scans with metastatic lesions, with the whole images from the twenty control group subjects. Uncorrected $P < 0.001$ was applied to identify patient-wise metabolically abnormal regions.

For each of the four comparisons, we also constructed a map of T-statistics and extracted the peak T values. As a proof-of-concept study, we investigated if the statistical analysis successfully revealed the metastatic lesions confirmed by the brain MRI previously.

Results

Extraction of the brain volume

The deep learning-based brain extractor successfully identified the existence of whole-brain volume, with the accuracy of 98% for the internal validation set. The performance of extracting the brain measured by the IOU of 3-D bounding boxes was 72.9±12.5% for the validation set. Using the predicted coordinates, all brains were successfully cropped and automatically normalized into the template space.

We show some representative images we applied for interval validation of the model in (**Fig. 2**). In both of the “torso” PET covering up to mid-thigh and “total-body” PET covering whole heights of body the extractor successfully located the brain (**Fig. 2a, b**). The extractor was also capable of identification of brain when the artifact caused by radiopharmaceutical injection was projected to the brain at the MIP image (**Fig. 2c**). When the brain volume was not fully included, the extractor classified the image as “not containing entire brain” (**Fig. 2d**).

Identification of brain metastasis from whole body FDG PET using the fully-automated brain analysis pipeline

The fully-automated brain extraction and quantitative analysis was applied to the patients with SCLC as a proof-of-concept study. The voxelwise T-test successfully identified the metastatic lesions in brain at three of four subjects in the case group ($P < 0.001$). In all of the three successful cases, the analysis revealed hypometabolic lesions due to edematous change around the lesion **(Fig. 3**). In the other case with unsuccessful result, the statistical analysis showed diffuse hypometabolism in frontoparietal lobe, instead of focal metabolic defect at the metastatic site (**Fig. 3**).

Discussion

Since the increased utilization of FDG-PET in neurologic disorders, many kinds of literature suggest methods for quantitative analysis for FDG-PET image of the brain [12, 21, 22] . However, most of the subjects with FDG-PET scan, especially oncologic patients, are not benefited from this kind of progress, for the lack of a handy and automated method of quantification. This work aims to achieve the first step of this automatization, by deep learning-based extraction of brain volume from the oncologic PET scan, which is followed by a scout quantitative analysis of the extracted brains. Fully-automated brain extraction and providing quantitative information in oncologic PET can be integrated into a system that warns of metastatic lesions or major brain diseases that can be overlooked in visual reading.

The key step of automated quantitative brain imaging analysis from the oncologic PET images was the extraction of brain volumes. For this purpose, we implemented the CNN-based deep learning model, which has been successful in solving a variety of problems in the field of image processing, including image classification, object detection and segmentation [23, 24], and vast portion of this success includes medical image processing [25, 26]. In most of the scans of internal validation, the automatic brain extractor based on ResNet-50 successfully identified the coverage of full brain in the whole-body scan and located and extracted the brain volume, even in the presence of artifact projected to the MIP image.

The extracted brain PET volume can be analyzed by many conventional quantitative analysis approaches. In this study, for the fully-automated process, we employed a spatial normalization process based on SyN algorithm implemented in DIPY package. Notably, the spatial normalization process after the brain extraction was fully automated. The spatially normalized brain can be further analyzed by quantitative softwares including SPM and 3-dimensional stereotactic surface projection (3D SSP) [27]. In this work, as a proof-of-concept study, we implemented SPM to identify metastatic lesions. This reveals the implication of the automatic brain extraction we performed, which could potentially extend to aid in the identification of unexpected metastasis during visual interpretation of oncologic PET study. Moreover, this method could be used to identify overlooked brain abnormalities such as dementia as well as tumorous lesions in the brain.

In the process of the quantitative analysis, as a proof-of-concept study, age matching was not performed between the metastatic subject and control group to yield rather non-specific decreased metabolism along the cerebral cortex in an elderly subject. This might have resulted from the physiologic decrease in gray matter volume accompanied by a normal aging process [28, 29]. Adjustment of patient factors (e.g., age and underlying disease) would be crucial to detect a localized metabolic disorder, apart from diffuse change of metabolism resulted from systemic condition.

Conclusions

Based on the deep learning-based model, we successfully developed a fully automated brain analysis method from oncologic FDG PET. The model could identify the existence of the brain volume, locate the contour of brain from the PET image, and perform the spatial normalization to the template. The quantitative analysis showed a feasibility of the identification of the metastatic brain lesion. We suggested that the model could be used to support FDG PET interpretation and analysis by finding unexpected brain abnormality including metastasis as well as brain disorders.

Abbreviations

FDG: Fluorodeoxyglucose

PET: Positron emission tomography

MIP: Maximal intensity projection

CNN: Convolutional neural network

SCLC: Small cell lung cancer

IOU: Intersection over union

MR: Magnetic resonance

SPM: Statistical parametric mapping

AD: Alzheimer's disease

SUV: Standardized uptake value

SyN: Symmetric normalization

SSP: Stereotactic surface projection

Declarations

Ethics approval and consent to participate

All procedures performed were in studies involving human participants were in accordance with the ethical standards of the institutional and/or national research committee and with the 1964 Helsinki declaration and its later amendments or comparable ethical standards (SNUH IRB No. 2104-046-1209).

Consent for publication

Not applicable.

Availability of data and material

Not applicable.

Competing interests

The authors declare that they have no competing interests.

Funding

This research was supported by the National Research Foundation of Korea (NRF-2019R1F1A1061412 and NRF-2019K1A3A1A14065446). This work was supported by the Korea Medical Device Development Fund grant funded by the Korea government (the Ministry of Science and ICT, the Ministry of Trade, Industry and Energy, the Ministry of Health & Welfare, the Ministry of Food and Drug Safety) (Project Number: 202011A06) and Seoul R&BD Program (BT200151).

Authors' contributions

H.C. designed this study. W.W. performed data collection, preparation, and statistical analysis. H.C. created software used in the work. J.C.P., G.J.C., K.W.K., and D.S.L. supported the result interpretation and discussion. All authors interpreted data results, drafted, and edited manuscript.

Acknowledgements

We thank our colleagues from Seoul National University Hospital, who provided insight and expertise that greatly assisted the research.

References

1. Almuhaideb A, Papathanasiou N, Bomanji J. 18F-FDG PET/CT imaging in oncology. Ann Saudi Med. 2011;31(1):3–13.
2. Zhu A, Lee D, Shim H, editors. Metabolic positron emission tomography imaging in cancer detection and therapy response. Seminars in oncology. Elsevier; 2011.
3. Fletcher JW, Djulbegovic B, Soares HP, Siegel BA, Lowe VJ, Lyman GH, et al. Recommendations on the use of 18F-FDG PET in oncology. J Nucl Med. 2008;49(3):480–508.
4. von Schulthess GK, Steinert HC, Hany TF. Integrated PET/CT: current applications and future directions. Radiology. 2006;238(2):405–22.
5. Kamel EM, Zwahlen D, Wyss MT, Stumpe KD, von Schulthess GK, Steinert HC. Whole-body 18F-FDG PET improves the management of patients with small cell lung cancer. J Nucl Med. 2003;44(12):1911–7.
6. Lee H-Y, Chung J-K, Jeong JM, Lee DS, Kim DG, Jung HW, et al. Comparison of FDG-PET findings of brain metastasis from non-small-cell lung cancer and small-cell lung cancer. Annals of nuclear medicine. 2008;22(4):281.
7. Tasdemir B, Urakci Z, Dostbil Z, Unal K, Simsek FS, Teke F, et al. Effectiveness of the addition of the brain region to the FDG-PET/CT imaging area in patients with suspected or diagnosed lung cancer. La radiologia medica. 2016;121(3):218–24.
8. Krüger S, Mottaghy MF, Buck KA, Maschke S, Kley H, Frechen D, et al. Brain metastasis in lung cancer. Nuklearmedizin. 2011;50(03):101–6.
9. Silverman DH, Dy CJ, Castellon SA, Lai J, Pio BS, Abraham L, et al. Altered frontocortical, cerebellar, and basal ganglia activity in adjuvant-treated breast cancer survivors 5–10 years after chemotherapy. Breast cancer research treatment. 2007;103(3):303–11.
10. Younes-Mhenni S, Janier M, Cinotti L, Antoine J, Tronc F, Cottin V, et al. FDG-PET improves tumour detection in patients with paraneoplastic neurological syndromes. Brain. 2004;127(10):2331–8.
11. Muzik O, Chugani DC, Juhász C, Shen C, Chugani HT. Statistical parametric mapping: assessment of application in children. Neuroimage. 2000;12(5):538–49.
12. Penny WD, Friston KJ, Ashburner JT, Kiebel SJ, Nichols TE. Statistical parametric mapping: the analysis of functional brain images. Elsevier; 2011.
13. Signorini M, Paulesu E, Friston K, Perani D, Colleluori A, Lucignani G, et al. Rapid assessment of regional cerebral metabolic abnormalities in single subjects with quantitative and nonquantitative [18F] FDG PET: a clinical validation of statistical parametric mapping. Neuroimage. 1999;9(1):63–80.

14. Kim YK, Lee DS, Lee SK, Chung CK, Chung J-K, Lee MC. 18F-FDG PET in localization of frontal lobe epilepsy: comparison of visual and SPM analysis. J Nucl Med. 2002;43(9):1167–74.
15. Ishii K, Willoch F, Minoshima S, Drzezga A, Ficaro EP, Cross DJ, et al. Statistical brain mapping of 18F-FDG PET in Alzheimer's disease: validation of anatomic standardization for atrophied brains. J Nucl Med. 2001;42(4):548–57.
16. Shofty B, Artzi M, Shtrozberg S, Fanizzi C, DiMeco F, Haim O, et al. Virtual biopsy using MRi radiomics for prediction of BRAf status in melanoma brain metastasis. Sci Rep. 2020;10(1):1–7.
17. ResNet-50. [Available from: https://keras.io/applications/#resnet50].
18. He K, Zhang X, Ren S, Sun J. Deep residual learning for image recognition. arXiv 2015. arXiv preprint arXiv:03385. 2015.
19. ImageNet. [Available from: http://www.image-net.org].
20. Garyfallidis E, Brett M, Amirbekian B, Rokem A, Van Der Walt S, Descoteaux M, et al. Dipy, a library for the analysis of diffusion MRI data. Frontiers in neuroinformatics. 2014;8:8.
21. Alf MF, Wyss MT, Buck A, Weber B, Schibli R, Krämer SD. Quantification of brain glucose metabolism by 18F-FDG PET with real-time arterial and image-derived input function in mice. J Nucl Med. 2013;54(1):132–8.
22. Kang KW, Lee DS, Cho JH, Lee JS, Yeo JS, Lee SK, et al. Quantification of F-18 FDG PET images in temporal lobe epilepsy patients using probabilistic brain atlas. Neuroimage. 2001;14(1):1–6.
23. Dhillon A, Verma GK. Convolutional neural network: a review of models, methodologies and applications to object detection. Progress in Artificial Intelligence. 2020;9(2):85–112.
24. Li Q, Cai W, Wang X, Zhou Y, Feng DD, Chen M, editors. Medical image classification with convolutional neural network. 2014 13th International Conference on Control Automation Robotics & Vision (ICARCV); 2014: IEEE.
25. Milletari F, Navab N, Ahmadi S-A, editors. V-net: Fully convolutional neural networks for volumetric medical image segmentation. 2016 fourth international conference on 3D vision (3DV); 2016: IEEE.
26. Winkler JK, Sies K, Fink C, Toberer F, Enk A, Deinlein T, et al. Melanoma recognition by a deep learning convolutional neural network—Performance in different melanoma subtypes and localisations. Eur J Cancer. 2020;127:21–9.
27. Minoshima S, Frey KA, Koeppe RA, Foster NL, Kuhl DE. A diagnostic approach in Alzheimer's disease using three-dimensional stereotactic surface projections of fluorine-18-FDG PET. J Nucl Med. 1995;36(7):1238–48.
28. Kalpouzos G, Chételat G, Baron J-C, Landeau B, Mevel K, Godeau C, et al. Voxel-based mapping of brain gray matter volume and glucose metabolism profiles in normal aging. Neurobiol Aging. 2009;30(1):112–24.
29. Yanase D, Matsunari I, Yajima K, Chen W, Fujikawa A, Nishimura S, et al. Brain FDG PET study of normal aging in Japanese: effect of atrophy correction. European journal of nuclear medicine molecular imaging. 2005;32(7):794–805.

Figures

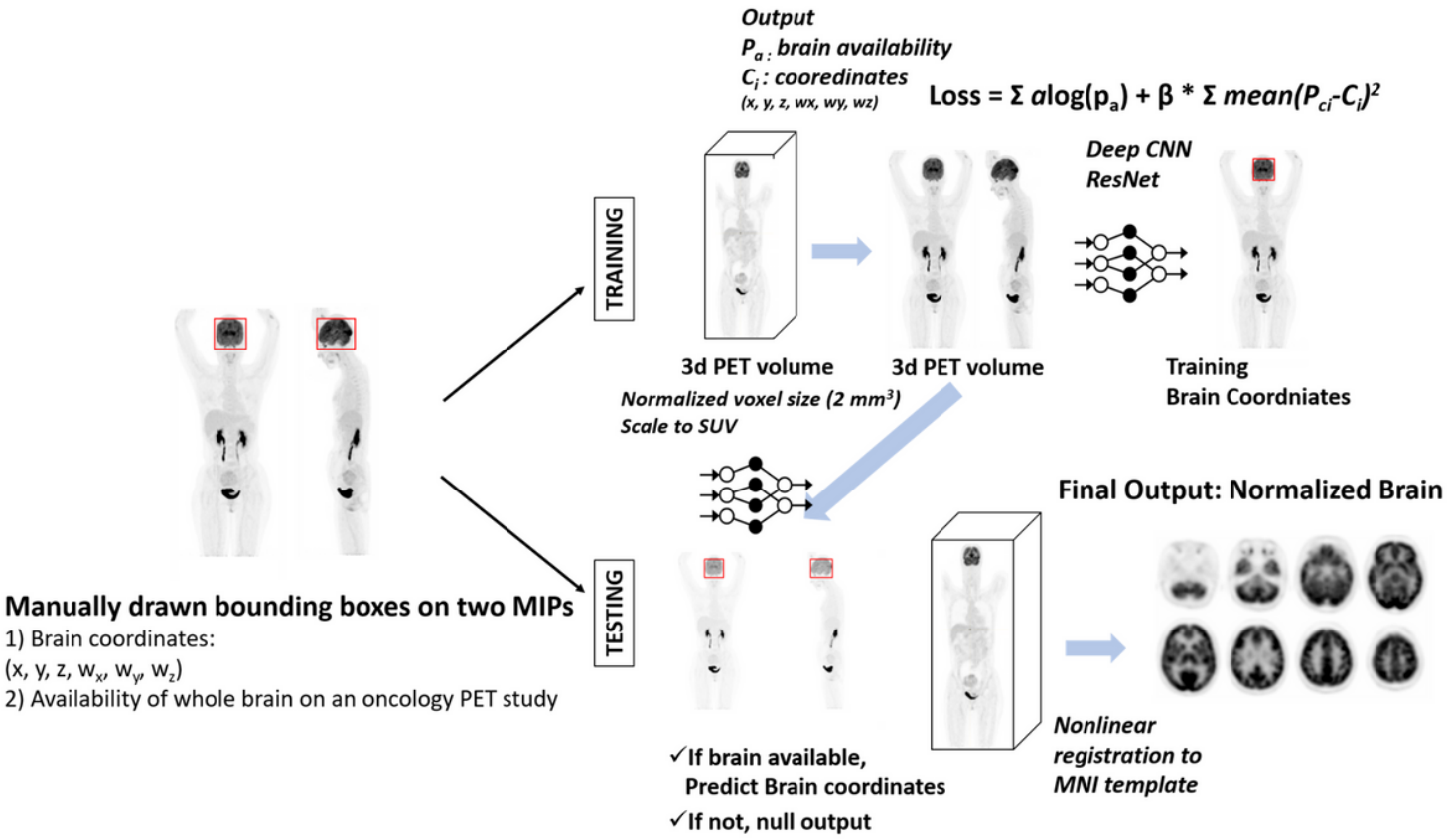

Figure 1

Brief outline of the automatic brain extraction. We trained the model with two manually drawn bounding boxes on maximal intensity projection (MIP) images. ResNet-50, a convolutional neural network (CNN) was used for learning model. Internal validation of model was performed. Finally, the brain volume was extracted and spatially normalized them to the template space, as mentioned later

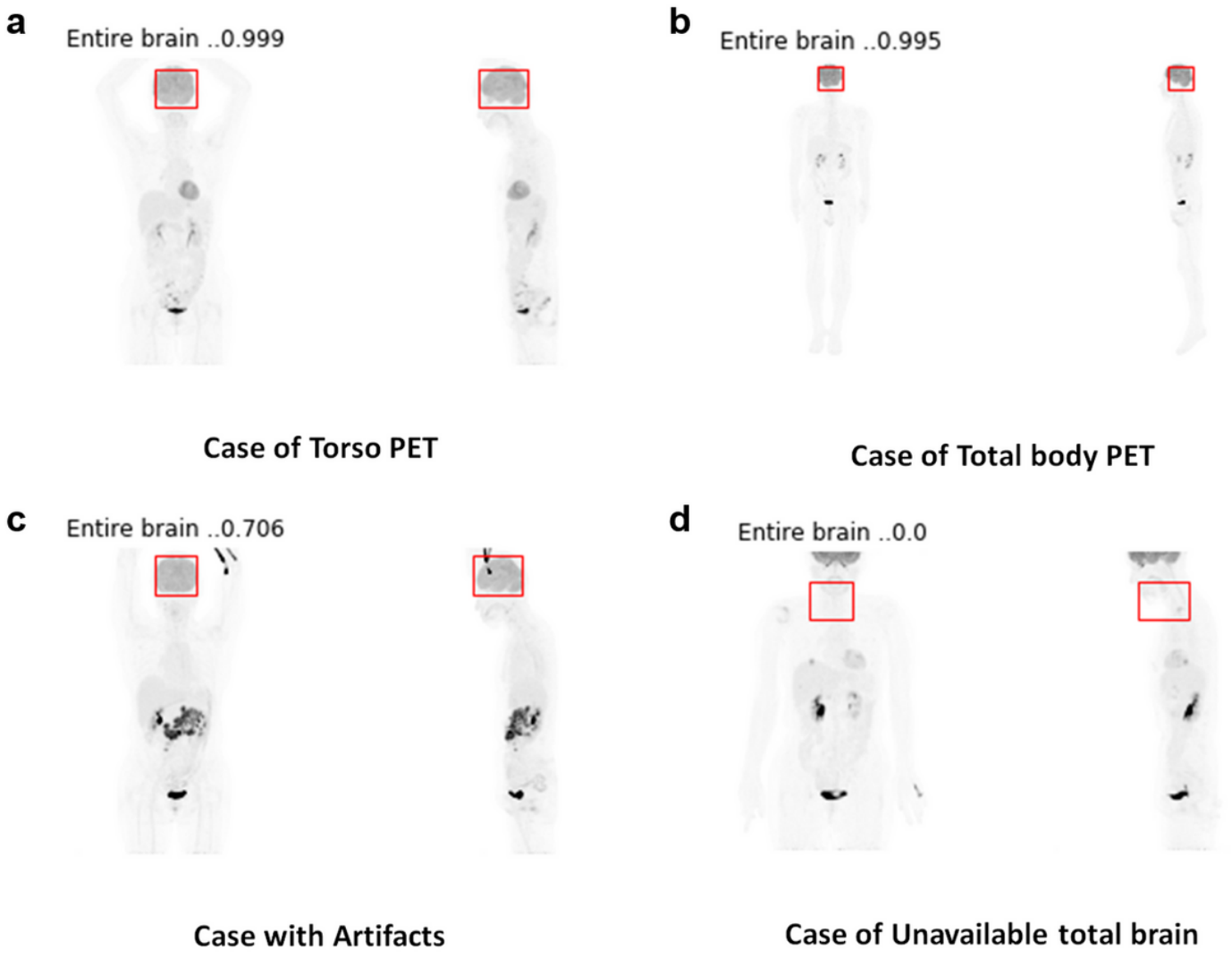

Figure 2

Representative results of the automatic brain extractor. (a, b) In both of the “torso” PET covering up to mid-thigh and “total-body” PET covering whole heights of body the extractor successfully located the brain. (c) The extractor was also capable of identification of brain when the artifact caused by radiopharmaceutical injection was projected to the brain at the MIP image. (d) When the brain volume was not fully included, the extractor classified the image as “not containing entire brain”.

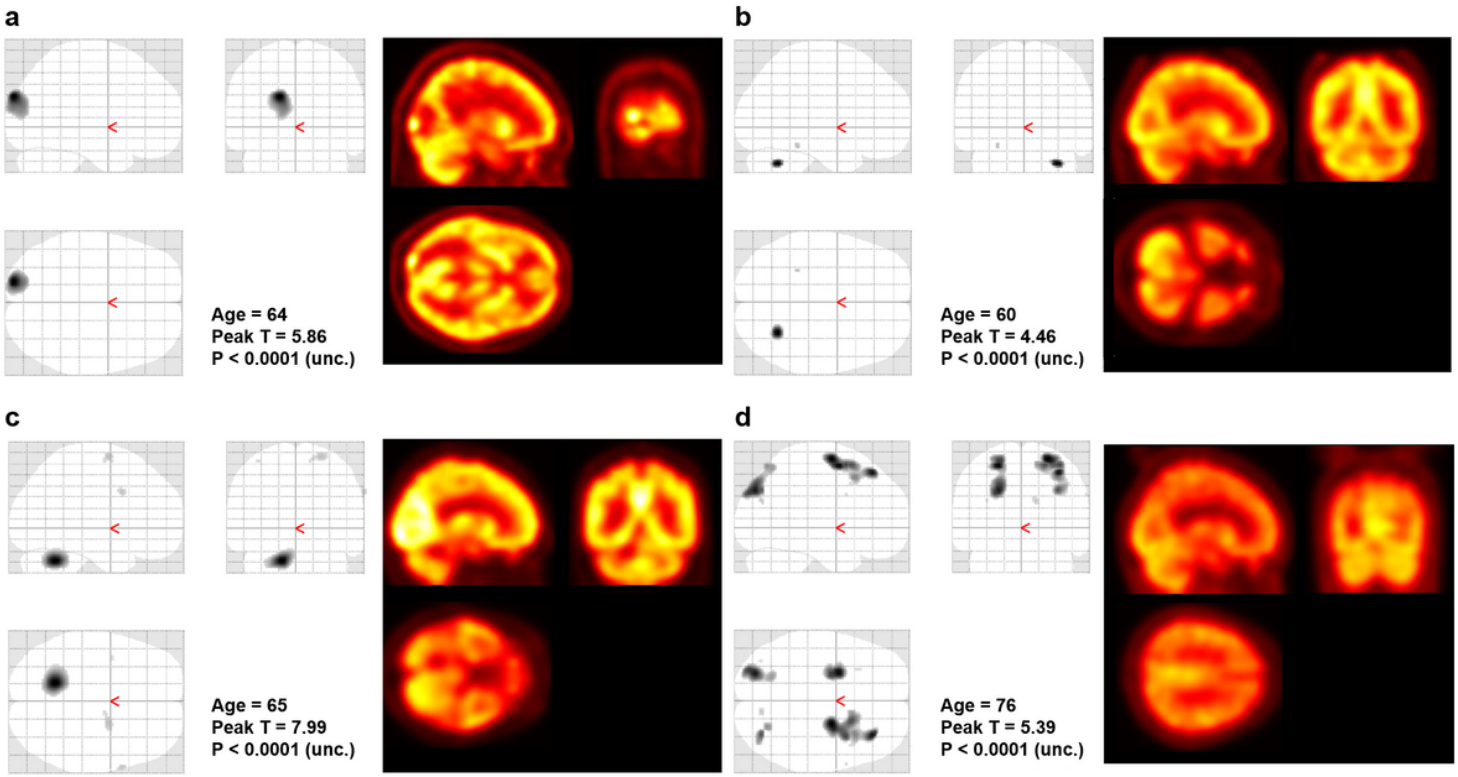

Figure 3

Quantitative analysis of the extracted brain. The voxelwise T-test successfully identified the metastatic lesions in brain at three of four subjects in the case group (uncorrected P < 0.001). The graphics on the left side show the brain regions that shows hypometabolism compared to the control group. The image on the right side shows the corresponding FDG-PET image. (a, b, c) In all of the three successful cases, the analysis revealed hypometabolic lesions due to edematous change around the lesion. (d) In the other case with unsuccessful result, the statistical analysis showed diffuse hypometabolism in frontoparietal lobe, instead of focal metabolic defect at the metastatic site.